F & S F 30593 revision

Title: Disruption of Protein Phosphatase 1 complexes using bioportides as a novel approach to target sperm motility

Running title: Sperm motility modulation by bioportides

Joana Vieira Silva, PhD [1,2,3], Maria João Freitas, PhD [1, a], Joana Santiago, MSc [1], Sarah Jones, PhD [4], Sofia Guimarães, PhD [1, b], Srinivasan Vijayaraghavan, PhD [5], Steven Publicover, PhD [6], Giorgio Colombo, PhD [7,8], John Howl, PhD [4*], Margarida Fardilha, PhD [1*]

[1] Laboratory of Signal Transduction, Department of Medical Sciences, Institute of Biomedicine – iBiMED, University of Aveiro, Aveiro, Portugal

[2] i3S- Instituto de Investigação e Inovação em Saúde, University of Porto, Porto, Portugal

[3] Laboratory of Cell Biology, Unit for Multidisciplinary Research in Biomedicine (UMIB), Institute of Biomedical Sciences Abel Salazar (ICBAS), University of Porto, Porto, Portugal

[4] Research Institute in Healthcare Science, University of Wolverhampton, Wulfruna Street, Wolverhampton, WV1 1LY, UK

[5] Kent State University, Kent State University, Kent, U.S.A.

[6] School of Biosciences, The University of Birmingham, Birmingham B15 2TT, UK

[7] University of Pavia, Department of Chemistry, Via Taramelli 12, 27100 Pavia, Italy

[8] SCITEC-CNR, Via Mario Bianco 9, 20131 Milano, Italy

* These authors contributed equally

Corresponding Author: Margarida Fardilha; Campus Universitario de Santiago, Agra do Crasto – Edificio 30, 3810-193 Aveiro, Portugal; Tel: +351 918143947. E-mail: mfardilha@ua.pt

[a] **Present address:** Laboratory of Protein Phosphorylation and Proteomics, Department of Cellular and Molecular Medicine, Faculty of Medicine, KU Leuven, Leuven, Belgium

[b] **Present address:** i3S- Instituto de Investigação e Inovação em Saúde, University of Porto, Porto, Portugal

Capsule

Endogenous proteomimetic sequences covalently coupled to cell penetrating peptides as sychnologically-organized bioportide constructs were successfully delivered to sperm cells to disrupt protein phosphatase 1 complexes and, consequently, reduce sperm motility.

Abstract

Objective: To design protein phosphatase 1 (PP1)-disrupting peptides covalently coupled to inert cell penetrating peptides (CPPs) as sychnologically-organized bioportide constructs as a strategy to modulate sperm motility.

Design: Experimental study.

Setting: Academic research laboratory.

Patients/Animals: Normozoospermic men providing samples for routine analysis and Holstein Frisian bulls.

Intervention(s): None.

Main Outcome Measure(s): Effect of the bioportides on the activity and interactions of PP1γ2 – a PP1 isoform expressed exclusively in testicular germ cells and sperm - and on sperm vitality and motility.

Results: PP1-disrupting peptides were designed based on the sequences from (i) a sperm-specific PP1 interactor (A kinase anchor protein 4, AKAP4) and (ii) a PP1 inhibitor (protein phosphatase inhibitor 2, PPP1R2). Those sequences were covalently coupled to inert CPPs as bioportide constructs, which were successfully delivered to the flagellum of sperm cells to induce a marked impact upon PP1γ2 activity and sperm motility. Molecular modelling studies further facilitated the identification of an optimized PP1 binding sequence and enabled the development of a Modified Stop Sperm (MSS1) bioportide with reduced size and increased potency of action. Additionally, a bioportide mimetic of the unique 22-amino acid C-terminus of PP1γ2 accumulated within spermatozoa to significantly reduce sperm motility and further define the PP1γ2-specific interactome.

Conclusion: These investigations demonstrate the utility of CPPs to deliver peptide sequences that target unique protein-protein interactions in spermatozoa to achieve a significant impact upon spermatozoa motility, a key prognostic indicator of male fertility.

Keywords

Sperm motility; Male contraception; Protein-protein interactions; Protein Phosphatase 1; PP1 disrupting peptides;

Introduction

The world's population has been rising at an alarming level and is expected to reach 9.8 billion by 2050 (1). Between 2010-2014, and despite the currently available contraceptive methods, approximately 40% of all pregnancies worldwide were unintended (2). Compared with female contraceptive measures, male contraceptive options are few in number and underused (3). To date, the development of new male contraceptives has mostly focused upon hormonal modulation (4); however, the pharmaceutical industry has abandoned many of the investments in this field due to reports of severe side effects (5). Most non-hormonal approaches in research focus either on the suppression of spermatogenesis or reversible physical barriers (3). The mechanism of sperm motility acquisition in the epididymis constitutes an ideal target for a new male contraceptive, since only post-testicular sperm maturation is affected, allowing normal hormone and spermatozoa production to occur and drugs do not necessarily need to cross the blood-testes barrier. In addition, drugs targeting sperm motility might also have a faster onset of action, allowing for administration immediately before intercourse (6).

The spermatozoon is virtually incapable of genetic expression. Any functional alteration (e.g. motility acquisition) in these cells depends on processes such as protein post-translational modifications (e.g. phosphorylation) (7). Protein phosphatase 1 (PP1) catalyses a considerable fraction of phosphoserine/threonine dephosphorylation reactions in eukaryotic cells and inhibition of its catalytic activity is essential for sperm motility acquisition and regulation (8–11). Smith et al showed immotile bovine caput epididymal sperm presented a two-fold higher activity of PP1 compared with fully mature motile sperm and that inhibition of PP1 by phosphatase inhibitors (calyculin A and okadaic acid) induced caput sperm motility (10,12).

In mammals, PP1 is encoded by three different genes giving rise to PP1α, PP1β and PP1γ isoforms. After transcription, PP1γ undergoes tissue-specific splicing, originating a ubiquitous isoform, PP1γ1, and a testis- and sperm-specific isoform, PP1γ2, which localizes at the posterior and equatorial head regions and along the entire flagellum (11,13,14). The molecular difference between these two PP1γ isoforms resides in the carboxyl-terminus (C-terminus) (15).

Regulation of PP1 catalytic activity is mediated by forming holoenzymes with regulatory interactors of protein phosphatase one (RIPPOs, previously called PP1-interacting proteins - PIPs) (16–21). In mammalian sperm, protein phosphatase inhibitor 2 (PPP1R2), a PP1 inhibitor, is central in controlling PP1 activity and, consequently, motility (7). In human mature sperm, part of the total PP1 population is bound to PPP1R2 and within these complexes PP1 is inactive (20). PPP1R2 is a highly intrinsically disordered protein that only acquires a defined structure when associated with PP1 (16,18,19). PPP1R2 contains two degenerated RVxF motifs (20,22). In mammalian sperm PP1γ2 appears to be the sole responsible for PP1 activity (10,11). and inhibition of PP1 by phosphatase inhibitors (calyculin A and okadaic acid) induces caput sperm motility (10).

A kinase anchor protein 4 (AKAP4) is a sperm-specific protein, previously described as a PP1γ2 interactor in human sperm (23) and associated with motility regulation (24). Male mice lacking AKAP4 are infertile, the motility of their sperm is poor, and the principal piece of the flagellum is morphologically and functionally abnormal (25). The *Akap4* gene knockout mice are also characterized by a significant change in the activity and phosphorylation status of PP1γ2 (26).

The interfaces between PP1γ2 and RIPPOs, such as PPP1R2 or AKAP4, represent an attractive target for pharmacological intervention to modulate PP1 and thus develop strategies to influence spermatozoa motility and male fertility. The binding of RIPPOs to PP1 is mediated by short amino acid (AA) motifs of which 10 have already been described and characterized (8,27,28). The most common PP1 binding motif, RVxF, is present in about 90% of all known RIPPOs and is thought to be the primary anchor point for subsequent interactions (27). The RVxF binding motif is a short linear motif that binds to the RVxF-binding site on PP1 and is unique to PP1 within the phosphoprotein phosphatase-like family (27,29). Currently only two drugs (salubrinal and trichostatin A) are known to modulate PP1 complexes (for review see (9)). In recent years, peptides have emerged as one of the important classes of therapeutic molecules but only a few *in vitro* studies have employed synthetic peptides (based on the RVxF motif) to disrupt PP1-RIPPOs

complexes (29–32). To date, modulation of spermatozoa physiology by synthetic peptides or small molecules that disrupt PP1 complexes has not been accomplished.

CPPs, mostly polycationic sequences of 12-20 AA in length, represent a very promising intracellular delivery system to target protein-protein interactions (PPIs) (33,34). In 2015, Jones et al demonstrated that CPPs are able to translocate into human and bovine sperm cells without detrimental influence upon viability or motility (33). More recently, a novel genre of CPP, distinct from conventionally inert vectors, has been developed that possesses the dual features of both cellular penetration and biological activity. Termed bioportides, these proteomimetic CPPs may include sequences derived from functional protein domains (e.g. RVxF binding motif) to serve as potent and selective biological modulators of PPIs (35–37).

In this study, we designed peptides mimetic of (i) the PP1 binding motif of human AKAP4, (ii) the PP1 binding motif of the human PPP1R2, and (iii) the unique 22-amino acid C-terminus of PP1γ2. These were covalently coupled to an inert CPP to form sychnologically-organized bioportide constructs with the aim of compromising PP1 interactions in intact spermatozoa. We rigorously evaluated the impact of these potential competitive bioportides on both PP1 activity and sperm motility. Additionally, we employed a bioportide (PP1γ2-CT) to characterize the PP1γ2 C-terminal interactome and identify proteins that specifically interact with the PP1γ2 isoform. This approach clarified the potential mechanism of action of this bioportide to further define the unique role of this PP1 isoform in human sperm.

Methods

Microwave-assisted solid phase peptide synthesis

Peptide mimetic sequences employed in the construction of bioportides (Table 1) included: (a) A 20 AA sequence from human AKAP4 including the PP1 binding motif (^{40}KVICF^{44}), AKAP4$^{33-52}$ (GQQDQDRKVICFVDVSTLNV; **AKAP4-BM**). (b) An Ala-substituted homologue of AKAP$^{43-52}$ lacking the PP1 binding motif (GQQDQDRAAAAAVDVSTLNV; **AKAP4-BMmut**). (c) A 19AA sequence from human PPP1R2 including an alternative PP1 binding motif (^{44}KSQKW^{48}), PPP1R2$^{36-54}$, (VDEELSKKSQKWDEMNILA; **PPP1R2-BM**). (d) A homologue of PPP1R2$^{36-54}$ with a scrambled PP1 binding motif (VDEELSKQWKKSDEMNILA; **PPP1R2-BMsc**). (e) The 22 AA C-terminus of human PP1γ2, PP1γ2$^{303-336}$, (KPNATRPVTPPRVASGLNPSIQKASNYRNNTVLY; **PP1γ2-CT**). (f) A shorter decapeptide homologue of AKAP4$^{33-52}$, YRSVITFVAV, designed by molecular modelling as an improved PP1 binding motif, was included as the N-terminus of **MSS1**. These endogenous sequences were covalently coupled to CPPs, penetratin or C105Y, as sychnologic bioportide constructs as indicated in Table 1.

Employing previously described protocols (38), AKAP4-BM, AKAP4-BMmut, PPP1R2-BM, PPP1R2-BMsc and PP1γ2-CT were prepared by microwave-assisted solid phase peptide synthesis using a Discover SPS Microwave Peptide Synthesizer (CEM Microwave Technology Ltd, Buckingham, UK) with fibre optic temperature control. These peptides were synthesized (0.1 mmol scale) using Rink amide MBHA resins pre-loaded with the first AA (AnaSpec, Inc., Cambridge Bioscience Ltd, Cambridge, UK) and employed a N-α-Fmoc protection strategy with HCTU activation. Deprotection with 7 ml of 20 % piperidine was performed for 3 min at 50 W/75 °C A majority of AA coupling reactions were accomplished with a 4-fold molar excess of Fmoc-protected AA with HCTU and diisopropylethylamine (DIPEA), molar ratio of 1:1:2 (AA/HCTU/DIPEA), in 4 ml for 10 min at 25 W/75 °C. Arg coupling was performed in two stages: 30 min 0 W/∼25 °C followed by 5 min at 17 W/75 °C. To reduce racemization of Cys coupling conditions were 5 min at 0 W/∼25 °C followed by 6 min at 17 W/50 °C with the hindered

base collidine (TMP) at a molar ratio of 1:1:2 (AA/HCTU/TMP; (39)). Aspartimide formation was reduced by the substitution of piperidine for 5 % piperazine and 0.1 M 1-hydroxybenztriazole hydrate (HOBt) in the deprotection solution. MSS1 was synthesized on a fully automated CEM Liberty Blue machine using similar activation and deprotection strategies routinely monitored by determining the UV absorption at 301 nm of Dibenzofulvene-piperidine adducts as recently described in detail (40).

Fluorescent peptides, to be used in cell imaging and quantitative uptake analyses, were synthesized by amino-terminal acylation with 6-carboxy-tetramethylrhodamine (TAMRA) (Novabiochem, Beeston, UK) as previously described (41). A biotinylated analogue of PP1γ2-CT, to be used in co-immunoprecipitation assays, was also synthesized using similar methods to conjugate biotin (Sigma) to the N-terminal of PP1γ2-CT. All peptides were purified by semi-preparative scale high-performance liquid chromatography and their predicted masses confirmed by mass spectrometry.

Phosphatase activity assay

A concentration range of commercial PPP1R2 (New England Biolabs, Herts, UK) was incubated with purified PP1γ2 (1:20; 1:200 and 1:2000) and either PPP1R2-BM or PPP1R2-BMsc for 30 min (ratio of 1:200:0.5 of PPP1R2, PP1γ2 and peptides). PP1γ2 activity was measured over 30 min, in 5 min intervals, using the SensoLyte® pNPP Protein Phosphatase Assay Kit *Colorimetric*(AnaSpec, Inc., Cambridge Bioscience Ltd, Cambridge, UK) and a PP1 specific assay buffer according to manufactures instructions. Negative control (only assay buffer) was included. Four replicas were performed.

Semen samples analyses and processing

This study was approved by the Ethics and Internal Review Board of the Hospital Infante D. Pedro E.P.E. (Aveiro, Portugal) (Process number:36/AO; Approved on 14 April 2015) and was conducted in accordance with the ethical standards of the Helsinki Declaration. Human semen

samples were obtained from a group of donors by masturbation into a sterile container. All donors signed informed consent allowing the samples to be used for scientific purposes. Basic semen analysis was performed according to World Health Organization (WHO) guidelines. Fresh semen from Holstein Frisian bulls was obtained from LusoGenes, LDA (Aveiro, Portugal). Semen was collected by artificial vagina and assessed by a certified veterinarian.

Human and bovine spermatozoa were isolated and washed from seminal plasma by centrifugation (500 g for 5 min, 3 times) using ALLGrade Wash medium (LifeGlobal, Brussels, Belgium). Spermatozoa pellets were resuspended in medium to a final concentration of $20x10^6$ cells/0.5 mL and incubated at 37 °C with 5 % CO_2 until the appropriated treatments were added.

Microscopic evaluation of the intracellular accumulation of the bioportides

Isolated bovine and human spermatozoa ($40x10^6$ cells) were resuspended and incubated with 10 μM tetramethylrhodamine (TAMRA)-labeled bioportides for 1 h at 37 °C in a humidified atmosphere of 5 % CO_2. Cells were then washed three times (500 g for 5 min) in ALLGrade Wash medium (LifeGlobal, Brussels, Belgium). To determine whether the fluorescently labeled bioportides were merely surface associated, we divided the sperm cell population in two and used a trypsin incubation to remove any surface associated bioportides. In summary, 50% of the cells were set aside ($20x10^6$ cells) and fixed in 4 % paraformaldehyde (PFA) for 20 min. The other 50% was incubated with 1 % (wt/vol) trypsin at 37 °C, collected by centrifugation at 3000 g, washed in ALLGrade Wash medium (LifeGlobal, Brussels, Belgium) and resuspended in 4 % PFA for 20 min. Fixed cells from each preparation were spread into coverslips and allowed to air dry. After mounting, slides were assessed by fluorescence microscopy (Imager.Z1, Axio-Cam HRm camera and AxioVision software, Zeiss, Jena, Germany).

Comparative quantitative analyses of bioportide translocation

The translocation efficacies of bioportides were determined by quantitative uptake analysis of fluorescently labeled peptides based upon the method previously described by Holm et al. (42). Isolated bovine and human spermatozoa were incubated with TAMRA-labeled bioportides at 37

°C in a humidified atmosphere of 5 % CO_2. Cells were then washed four times with 200 µl of phosphate buffered saline (PBS) (600 g for 5 min), detached with 1 % (w/v) trypsin at 37 °C, collected by centrifugation at 3000 g and lysed in 300 µl 0.1 M NaOH for 2 h on ice. 250 µl of each sample cell lysate were transferred to a black 96-well plate and analysed using an Infinite® 200 PRO (Tecan, Switzerland) (λAbs 544 nm/λEm 590 nm).

Cell viability assays

Bovine spermatozoa viability was evaluated using the Trypan Blue viability test (Fisher Scientific, Loures, Portugal) according to manufacturer's guidelines. 200 sperm cells were counted per replicate using a Zeiss Primo Star microscope (Zeiss, Jena, Germany). Human spermatozoa viability was measured using the CellTiter 96® AQueous Non-Radioactive Cell Proliferation Assay (Promega, Madison, USA) according to manufacturer's guidelines. The reduction of tetrazolium compounds has previously been used as a reliable and rigorous assessment of spermatozoa viability (43).

Motility assays

Bovine and human sperm cells were diluted in medium to achieve a total volume of 500 µl, containing $20x10^6$ sperm cells. Control samples included sperm cells in medium alone. The influence of bioportides upon sperm motility parameters was assessed using the Sperm Class Analyzer CASA System (Microptic S L, Barcelona, Spain) with SCA® v5.4 software. Samples and controls (2 µl) were loaded into individual chambers of Leja Standrat Count 8 chamber slide 20 µm depth (Leja Products B. V., The Netherlands) (bovine) or Leja Standrat Count 4 chamber slide 10 µm depth (Leja Products B. V., The Netherlands) (human), which were pre-heated at 37 °C. This temperature was maintained while at least 1000 sperm cells per measurement were evaluated. Each bioportide was tested on samples from 3 individual donors and all the conditions were performed in triplicate.

Computer-assisted peptide design and optimisation

To support the design of chemically optimised bioportides, molecular dynamics simulations (MD) were initially used to characterise possible conformational preferences of the PP1γ2 protein target and of a prototypical binding sequence derived from AKAP4. PP1γ1 was retrieved from Protein Data Bank (PDB codes: 2O8G) and used as a target for peptide-binding since the crystal structure of PP1γ2 is not available. PP1γ1 is highly homologous to PP1γ2 and differs only by the lack of a long and disordered carboxyl tail, a structural feature expected to introduce a high level of noise in MD simulations. Further, the RVxF binding pocket of PP1γ1 and PP1γ2 are identical. The peptide sequence studied in isolation was AKAP4wt (QRKVICFVAV). Each MD was performed using the Amber 14 (44), suite of programs. The peptide and protein were simulated using ff14SB (45) force field and prepared with Leap to add missing hydrogen atoms and to generate a solvated system. The simulation box of explicit water molecules (TIP3P model) was extended up to 10 Å (PP1γ) or 12 Å (AKAP4 peptide), counter ions of Na^+ were added to neutralize the system. The simulation started with an unrestrained minimization consisting of 2500 steps followed by a minimization constrained at the Ca of 4000 steps. The minimized system was then equilibrated in two cycles at 300K: the first keeping the peptide under a restraint at Ca constant force of 500 kcal/mol/A^2 and the second equilibration with the release of the restraint for 5 ns. Simulations with constant temperature (298K), using the weak-coupling algorithm (46). The SHAKE algorithm was used to constrain all covalent bonds involving hydrogen atoms. The production runs for both the protein and the peptide were 500 ns long.

For each system, a conformational cluster analysis using gromos algorithm was carried out using a cut-off of 0.2 nm (47). Each of the cluster centroids is used as a representative structure. The representative structures of the most populated clusters for the protein and the peptide were used as inputs for protein-peptide docking experiments using the GLIDE peptide-docking module of the MAESTRO suite of programs. The best solution was used for further refinement of the peptide sequence.

Sequence optimisation for binding to PP1γ1 was carried out using PinaColada and PepCrawler. Briefly, the principle behind PinaColada lies on the optimisation of the initial peptide through the

ant-colony method (48). To refine the peptide with the highest inhibitory affinity the peptide conformation and free energy of the interaction with the receptor protein is predicted through the PepCrawler algorithm (49), a local docking algorithm for peptide-protein interactions. Five runs were performed from which the top 4 best performers were selected for further synthesis. This selection was based on the lowest energy and funnel which together provide both the best binding energy and binding affinity.

MD simulation studies of PPP1R2-BM and scrambled and the 7 flanking AA were performed by the MD simulation package Amber v14 applying Amber-ff14SB force field (45). The two systems were solvated, in a simulation octahedral box of explicit water molecules (TIP3P model) (50), counter ions were added to neutralize the system and periodic boundary conditions imposed in the three dimensions (12 Aº). After minimizations, systems were subjected to an equilibration phase where water molecules position were restrained, then unrestrained systems were simulated for a total of 5 microseconds, in a NPT ensemble; Langevin equilibration scheme and Berendsen thermostat were used to keep constant temperature (300 K) and pressure (1 atm), respectively. Electrostatic forces were evaluated by Particle Mesh Ewald method and Lennard-Jones forces by a cutoff of 10 Å. All bonds involving hydrogen atoms were constrained using the SHAKE algorithm. Structural and graphical representations were carried out using VMD and prepared in Maestro (51). Simulations were run for 200 ns in each system.

Blot overlay

Recombinant PP1γ2 protein was resolved by SDS-PAGE and transferred onto a nitrocellulose membrane that was incubated with either recombinant AKAP4 protein (25 pmol/mL) (ab152924, Abcam, Cambridge, MA, USA) or MSS1 peptide (500 pmol/mL) and recombinant AKAP4 protein (25 pmol/mL) (ab152924, Abcam, Cambridge, MA, USA). After washing to remove excess protein, bound AKAP4 was detected by incubating the membrane with a mouse anti-AKAP4 antibody (ab56551, Abcam, Cambridge, MA, USA). Immunoreactive bands were revealed by incubation with an Infrared IRDye-labeled anti-mouse secondary antibody using the

Odyssey Infrared Imaging System (LI-COR Biosciences, US). Ponceau S was used as the protein-loading control.

Co-immunoprecipitation of biotinylated PP1γ2-CT peptide in human spermatozoa

To identify the interactome of the unique C-terminus of PP1γ2 in human spermatozoa, a co-immunoprecipitation of the biotinylated PP1γ2-CT peptide was performed. 15×10^6 human sperm cells were incubated with 5 µM of biotinylated PP1γ2-CT peptide for 15 min at 37°C in a humidified atmosphere of 5% CO_2. Negative controls contained no peptide. Sperm cells were collected by centrifugation (600g for 15 min) and lysed in 250 µl of 1x RIPA buffer (0.5M Tris-HCl, pH 7.4, 1.5M NaCl, 2.5% deoxycholic acid, 10% NP-40, 10mM EDTA) (Millipore Iberica S.A.U., Madrid, Spain) supplemented with protease inhibitor (1 mM PMSF) for 30 minutes on ice and centrifuged at 16000g for 15 min at 4ºC. 90% of the supernatant (sperm soluble fraction) was used for the subsequent steps. 10% of the soluble fraction was saved and the pellet (sperm insoluble fraction) was re-suspended in 250 µl 1% SDS. 50 µl of Dynabeads® M-280 Streptavidin (Life Technologies AS., Madrid, Spain) were added to the RIPA supernatant extracts and incubated for 30 min at room temperature with gentle rotation. After incubation, the supernatant was removed to a new tube and stored (unbound IP fraction). The beads were washed three times with 1 ml trypsin digestion buffer (20 mM Tris-HCl pH 8.0, 2 mM $CaCl_2$) (for LC-MS/MS). After washing, the beads were re-suspended in 150 µl trypsin digestion buffer (20 mM Tris-HCl pH 8.0, 2 mM $CaCl_2$) and stored at -20°C until intensity-based label-free quantitative (LFQ) LC-MS/MS analysis. The experiment was performed in triplicate.

Sample preparation and LC-MS/MS analysis

A total of 6 samples were prepared for LC-MS/MS analysis. Washed beads were re-suspended in 150 µl digestion buffer and incubated for 4 h with 1 µg trypsin (Promega) at 37 ˚C. Beads were removed, another 1 µg of trypsin was added and proteins were further digested overnight at 37 ˚C. Peptides were purified on Omix C18 tips (Agilent), dried and re-dissolved in 20 µl loading

solvent A (0.1% trifluoroacetic acid in water/acetonitrile (ACN) (98:2, v/v)) of which 2 µl was injected for LC-MS/MS analysis on an Ultimate 3000 RSLCnano system (Thermo) in line connected to a Q Exactive mass spectrometer (Thermo). Trapping was performed at 10 µl/min for 4 min in loading solvent A on a 20-mm trapping column (made in-house, 100-µm internal diameter (I.D.), 5-µm beads, C18 Reprosil-HD, Dr. Maisch, Germany) and the sample was loaded on a 150-mm analytical column (made in-house, 75-µm I.D., 3-µm beads C18 Reprosil-HD, Dr. Maisch). The Ultimate 3000's column oven was set to 35°C. For proper ionization, a fused silica PicoTip emitter (10 µm inner diameter, New Objective) was connected to the analytical. Peptides were eluted by a linear increase from 2 to 55% MS solvent B (0.1% FA in water/ACN (2:8, v/v)) over 120 min, at a flow rate of 300 nl/min, followed by a 5-miN washing phase plateauing at 99% MS solvent B and a re-equilibration phase for 32 min with 98% MS solvent A (0.1% FA in water) adding up to a total run length of 160 min. The mass spectrometer was operated in data-dependent, positive ionization mode, automatically switching between MS and MS/MS acquisition for the 5 most abundant peaks in a given MS spectrum. The source voltage was 4.5 kV, and the capillary temperature was 275°C. One MS1 scan (m/z 400−2,000, AGC target 3×10^6 ions, maximum ion injection time 80 ms), acquired at a resolution of 70,000 (at 200 m/z), was followed by up to 5 tandem MS scans (resolution 17,500 at 200 m/z) of the most intense ions fulfilling predefined selection criteria (AGC target 5×10^4 ions, maximum ion injection time 80 ms, isolation window 2 Da, fixed first mass 140 m/z, spectrum data type: centroid, underfill ratio 2%, intensity threshold 1.3 x 10^4, exclusion of unassigned, 1, 5-8, >8 positively charged precursors, peptide match preferred, exclude isotopes on, dynamic exclusion time 12 s). The HCD collision energy was set to 25% Normalized Collision Energy and the polydimethylcyclosiloxane background ion at 445.120025 Da was used for internal calibration (lock masses).

LC-MS/MS data analyses

Data analysis was performed with MaxQuant (version 1.5.7.4) using the Andromeda search engine with default search settings including a false discovery rate set at 1% on both the peptide and protein level. Spectra were searched against the SwissProt human database (from January

2017 with 20,172 entries). The mass tolerance for precursor and fragment ions was set to 4.5 and 20 ppm, respectively, during the main search. Enzyme specificity was set to C-terminal of arginine and lysine, also allowing cleavage next to prolines with a maximum of two missed cleavages. Variable modifications were set to oxidation of methionine residues, phosphorylation of serine, threonine and tyrosine as wells as acetylation of protein N-termini. Matching between runs was enabled with a matching time window of 1 minute and an alignment time window of 20 min. Only proteins with at least one unique or razor peptide were retained leading to the identification of 629 proteins. Proteins were quantified by the MaxLFQ algorithm integrated in the MaxQuant software. A minimum ratio count of two unique or razor peptides was required for quantification. Further data analyses were performed with the Perseus software (version 1.5.5.3) after uploading the protein groups file from MaxQuant. Reverse database hits were removed and replicate samples were grouped. Proteins with less than three valid values in at least one group were removed and missing values were imputed from a normal distribution around the detection limit resulting in 463 quantified proteins, which were subsequently used for further data analysis. These quantified proteins were subjected to a two-sided, unpaired t-test using permutation-based muliparameter correction with 1000 randomisations and a false discovery rate of 1%. The results of this t-test are shown in the volcano plot in Supplementary Figure 1 and listed in Supplemental Table 15. For each protein, the log2 (CT/NCT) fold change value is indicated on the X-axis, while the statistical significance (-log p value) is indicated on the Y-axis. Proteins outside the curved lines, set by an FDR value of 0.01 and an S0 value of 1 in the Perseus software, represent specific PP1γ2-CT interaction partners.

Bioinformatic Analysis: Gene Annotation and Involvement in Male Infertility-Related Phenotypes

The UniProt database was used to collect information regarding molecular function and the Human Protein Atlas (HPA) database (available from www.proteinatlas.org) was used to retrieve information regarding tissue expression and subcellular location (data was downloaded on 23/01/2020). The databases DisGeNET (curated gene-disease associations list downloaded on

06/2019) and Disease (data downloaded on 06/2019) were explored to identify proteins associated with male infertility phenotypes. Proteins associated with defects in male fertility were also obtained from the Jackson Laboratories mouse knockout database - MGI (data downloaded on 06/2019). The HIPPIE database was used for retrieving human PPI data (downloaded 07/2019). This database is regularly updated by incorporating interaction data from major expert-curated experimental PPI databases (such as Bell09, BioGRID, HPRD, IntAct, and MINT). Network analyses were performed using Cytoscape (version 3.6.0) (52) (Institute for Systems Biology and International Consortium of Open Source Developers, Seattle,Washington, USA).

Statistical analyses

Descriptive statistics of all data were calculated. To determine the *in vitro* effect of the bioportides on PP1 activity, for each condition (11 conditions), a Pos Hoc analysis of the Friedman test to detect differences over time (pairwise comparisons) was performed. For each time (0 m, 5 m, 15 m, 20 m, 25 m and 30 m), the Kruskall Wallis test was used to detect differences between the conditions (independent groups). Finally, a pairwise comparison of conditions test was applied to identify between differences (Mann-Whitney U test). The statistical significance of the effect of the exposure of bioportides on human and bovine spermatozoa motility and vitality was calculated with Mann Whitney U-tests. The significance level was set at 0.05.

Results

The AKAP4-BM bioportide translocates into spermatozoa to negatively impact upon spermatozoa motility

A lead disruptive AKAP4-BM bioportide comprising the PP1 binding motif RVxF in AKAP4 (^{40}KVICF^{44}) and flanking sequences was designed (Table 1). A bioportide with penta-alanine substituted for the PP1 binding motif of AKAP4 (AKAP4-BMmut) was used as control. Fluorescent microscopy confirmed the intracellular accumulation of both AKAP4-BM and AKAP4-BMmut bioportides within human (Figure 1 a) and bovine spermatozoa. Quantitative analyses demonstrated that, even at time zero, corresponding to the addition of the bioportides to spermatozoa and immediate washing to remove the bioportide containing solution, the AKAP4-BM bioportide had entered the sperm cells (Figure 1 b). Intracellular accumulation of AKAP4-BM increased with both time- and concentration-dependent kinetics (Figure 1 b). The intracellular uptake of AKAP4-BMmut did not increase over time and exposure to increasing concentrations of this bioportide revealed a saturation at 7.5 μM (Figure 1 b). These differences in uptake efficacy may be explained, at least in part, by an intact RVxF motif in AKAP4-BM specifically interacting with intracellular sperm proteins.

The percentage of viable human spermatozoa was not significantly altered after treatment with 10 μM bioportides, except by the 2h incubation with the AKAP4-BM bioportide where a decrease was observed (Figure 1 c and Supplementary Table 1; similar results were observed in bovine spermatozoa, Supplementary Table 3). A significant decrease in sperm vitality was observed at a 20 μM exposure of the AKAP4-BM bioportide (Supplementary Table 3).

Exposure of human sperm to AKAP4-BM bioportide induced a significant decrease in both fast and slow progressive motility and an increase in the percentage of immotile spermatozoa in comparison with both the negative control and the mutated bioportide (Figure 1 d ; Supplementary Tables 1 and 2; similar results were observed in bovine spermatozoa, Supplementary Tables 3 and 4). There was no time-dependent effect of the AKAP4-BM bioportide in any motility parameter (Supplementary Table 4).

Computational studies of the AKAP4/PP1γ interaction enabled the design of an optimised bioportide

To increase the potency of action of the AKAP4-BM bioportide, computational modelling studies were performed. First, the structural dynamics of protein target (PP1γ) was studied by means of all atom MD simulations to explore protein conformations and variations in the shapes of binding pocket on the surface of the target. The main conformations sampled by the protein in this timespan were characterized by cluster analysis. One major cluster, containing more than 90% of the structures, was identified. The representative structure of this cluster was then used as a target for further docking and peptide-design studies (Figure 1 e). Specifically, our attention was focused on the RVxF binding pocket, which is unique to PP1 within the phosphoprotein phosphatase-like and is the primary anchor point for most RIPPOs. RVxF features residues were 161, 164, 237, 238, 250, 252, 256, 259, 261, 278, 283, 284, 286, 288, 290, 291. Root Mean Square Fluctuation (RMSF) analysis of the pocket indicates a high structural stability for this substructure (Figure 1 f).

As no crystal structure of AKAP4 is available, we performed MD simulation based on part of the sequence of the AKAP4-BM bioportide (QRKVICFVAV - labeled here as AKAP4wt) to investigate its structural preferences. 500 ns simulation was carried out. The most representative cluster structure (35%) was retrieved for further docking. The representative structure of the most populated conformational cluster was used as target structure for docking. Next, the most favourable docking pose obtained from the previous docking experiment was used as a template to generate optimised sequences using the PinaColada (53) approach. Once an optimised sequence hypothesis was obtained, the latter was further refined using the PepCrawler algorithm (Donsky and Wolfson, 2011). PepCrawler rapidly generates large amounts of flexible peptide conformations, allowing backbone and side chain flexibility. A binding energy funnel score was used to evaluate the protein–peptide complexes binding affinity. On this basis, we selected the best performer for further synthesis: AKAP4_Pep3: **Y**R**S**VI**T**FVAV (Figure 1 g; Supplementary Table 5). This approach enabled the design of an optimised Modified Stop Sperm (MSS1) bioportide, based on AKAP4_Pep3 (Table 1).

The MSS1 bioportide disrupts PP1γ2/AKAP4 interaction to significantly decrease spermatozoa motility

The disruption of PP1γ2/AKAP4 interaction by the MSS1 bioportide was demonstrated by blot overlay. Recombinant PP1γ2 protein was resolved by SDS-PAGE and the membranes were incubated with either recombinant AKAP4 protein (25 pmol/mL) or MSS1 bioportide (500 pmol/mL) plus recombinant AKAP4 protein (25 pmol/mL). After washing to remove excess protein, bound AKAP4 was detected by incubating the membrane with a mouse anti-AKAP4 antibody. Increased quantities of recombinant PP1γ2 protein resulted in proportionately increased amounts of AKAP4 binding, thus demonstrating its specific interaction with AKAP4 (Figure 1 h). Incubation with the MSS1 bioportide reduced the amount of AKAP4 protein bound to PP1γ2 (Figure 1 h).

Exposure of human spermatozoa to MSS1 induced a significant decrease in both fast and slow progressive motility and an increase in the percentage of immotile spermatozoa in comparison with both the negative control and the mutated bioportide (Figure 1 i and j; Supplementary Tables 6 and 7). No significant alterations were observed in non-progressive motility (Supplementary Table 7). Application of the mutated AKAP4-BM did not lead to significant differences in motility parameters in comparison with the negative control (Figure 1 i and j; Supplementary Table 7). There were no significant differences between the time points tested (15 min and 1h) at 10 μM exposure in any motility parameter (Supplementary Table 7). The percentage of viable spermatozoa was not significantly changed after treatment with the MSS1 bioportide at the concentrations tested (Supplementary Table 6 and 7). A decrease in sperm vitality began to be observed with a 20 μM exposure of the MSS1 bioportide.

PPP1R2 bioportide modulates PP1γ2 activity and spermatozoa motility

To assess the disruptive capacity of peptides designed based on a potent PP1 inhibitor (PPP1R2) RVxF motif, PP1 activity was evaluated in the presence of PPP1R2 and the PPP1R2-BM or

PPP1R2-BMsc peptides. Figure 2 a shows that PPP1R2 inhibited PP1γ2 in a concentration dependent manner (PPP1R2 alone does not present any phosphatase activity (data not shown)). After 15 min incubation PPP1R2 significantly inhibited approximately 50% of PP1γ2 activity, an effect that persisted up to at least 30 min incubation (Figure 2 a, Supplementary Table 8 and 9). Upon adding PPP1R2-BM, PP1γ2 activity was restored to original values starting at 15 min (Figure 2 a). PP1γ2 activity was also restored by PPP1R2-BMsc addition (time point 25 min and 30 min) (Figure 2 a). These results prove that PPP1R2-BM bioportides disrupt the PP1γ2/PPP1R2 complex, *in vitro*, and consequently restore PP1γ2 activity.

Fluorescent cell imaging analysis revealed that fluorescently labeled PPP1R2-BM and PPP1R2-BMsc (10μM) were able to translocate and accumulate in human and bovine sperm (Figure 2 b). Quantitative uptake comparisons demonstrated that PPP1R2-BM presents a higher cellular uptake, when compared with PPP1R2-BMsc (human 2.9 times; bovine 10.7 times) (Figure 2 c). Between human and bovine spermatozoa the accumulation pattern of both bioportides is similar. Higher concentrations were also analysed (20μM and 50 μM) and the pattern of bioportide distribution was similar (data not shown).

Concerning the effect of PPP1R2-BM on sperm motility, exposure of bovine sperm to 100 μM PPP1R2-BM reduced significantly the percentage of progressive fast motile sperm at 1 h and 2 h compared with the negative control (Figure 2 e). In contrast, the percentage of immotile sperm increased significantly in both timepoints tested (Figure 2 e, Supplementary Table 10 and 11). PPP1R2-BMsc presented a similar effect (Figure 2 e). No significant alterations were observed in slow progressive motility, non-progressive motility and vitality (Figure 2 d; Supplementary Table 11).

Computational studies of the PPP1R2-BM bioportides

Molecular dynamics simulations were performed with the PPP1R2-BM peptide sequence, which comprised the PPP1R2 RVxF binding motif and 7 AA flanking at N- and C-termini. Figure 2 f and e shows that the RVxF binding motif forms a rigid secondary structure, an α-helix, while the

remaining sequence showed no secondary structure. In the case of PPP1R2-BM peptide, the most frequent cluster presented a pronounced α-helix at the N-terminus and a tendency to form a α-helix at the C-terminus. The middle region, comprising the scrambled RVxF binding motif (QWKKSD), showed no evident secondary structure with an apparently higher flexibility (Figure 2 f and g). Next, AA substitution studies using previous crystallography studies (PDB code 2O8G) revealed that the peptide with PPP1R2 RVxF scrambled may bind more stably and with more affinity with the core region of the PP1 RVxF pocket. The substitution of lysine to a glutamine in the first AA of RVxF motif appears to provide more stability to the peptide, while the change in the second AA from a serine to a tryptophan confers more affinity to the PP1 RVxF pocket (Figure 2 h). In view of these results, it is possible to envisage that a higher degree of structural preorganization correlates with better observed activity.

The PP1γ2-CT bioportide translocates into spermatozoa with a negative impact on motility

A peptide sequence that mimics the unique 22-amino acid C-terminus of PP1γ2 (PP1γ2-CT) and is conserved in both bovine and human proteins was used to compromise the isoform-specific interactions between PP1γ2 and its interactors.

Fluorescent microscopy revealed the intracellular accumulation of the PP1γ2-CT bioportide in human (Figure 3 a) and bovine spermatozoa. Quantitative analysis demonstrated that at time zero, corresponding to the addition of the bioportides and immediate washing to remove the bioportide containing solution, the PP1γ2-CT bioportide had already entered sperm cells, revealing its rapid intracellular translocation (Figure 3 b). Additionally, bioportide uptake increased over time (Figure 3 b). Exposure of spermatozoa to increasing concentrations of the PP1γ2-CT bioportide was followed by increasing intracellular translocation (Figure 3 b).

The percentage of viable spermatozoa, both human and bovine, was not significantly changed after treatment with the bioportide (Figure 3 c; Supplementary Table 12 and 13). Exposure of human spermatozoa to PP1γ2-CT induced a significant decrease in both fast and slow progressive motility and an increase in the percentage of immotile spermatozoa (Figure 3 d and e;

Supplementary Table 2 and 12). Similar results were observed in bovine spermatozoa (Supplementary Table 14). No significant alterations were observed in non-progressive motility in both bovine and human samples (Supplementary Table 2 and 14). There were no significant differences between the concentrations tested (5, 10 and 20 μM) in any motility parameter (Supplementary Table 14). Moreover, there was no time-dependent effect on motility of the PP1γ2-CT bioportide for the conditions tested (Supplementary Table 14). Both PP1γ2-CT and TAMRA- PP1γ22-CT induced a similar effect on sperm motility parameters, revealing that the fluorescent labelling did not affect significantly the peptide's action (Supplementary Table 14).

PP1γ2 C-terminus interactome

To identify proteins that specifically interact with the 22-amino acid C-terminus of the human PP1γ2, human spermatozoa were incubated with a biotinylated PP1γ2-CT (B-PP1γ2-CT) bioportide and a co-immunoprecipitation of the peptide was performed followed by LC-MS/MS analyses. Two peptides that matched with the PP1γ2-CT peptide sequence were identified (Supplementary Table 15) which indicates bait recovery after pull down. No peptides corresponding to PP1γ2-CT were identified in the negative control.

Mass spectrometric data revealed 73 proteins upregulated in samples incubated with the peptide when compared with the negative controls (Supplementary Table 16). Interactors were identified using a student's t-test comparing the LFQ intensities of all proteins identified in replicates of CT with the LFQ intensities of all proteins identified in the control. Proteins were classified as interactors according to their position in the volcano plot. When log2(CT/NC) and -log(p-value) were plotted against each other in a volcano plot the unspecific background binders appears around zero. The interactors appear on the right side of the volcano plot and the higher the difference between the group means and the p value the more the interactors move to the top right corner of the plot, which is the area of highest confidence for a true interaction. Among these 73 proteins, 23 proteins were classified as possible contaminants and consequently excluded (e.g. 22 ribosomal proteins and one extracellular matrix glycoprotein). Previous findings indicate that

ribosomal proteins have high affinity to the magnetic beads (54). Only proteins that were quantified in at least 3 replicates of one of both conditions were considered.

Thus, we identified 50 proteins that interact with the 22-amino acids C-terminus of human PP1γ2 (Supplementary Table 16).

Network of the PP1γ2 C-terminus interactome

A protein-protein interaction (PPI) network was constructed with the proteins identified as PP1γ2-CT interactors (Figure 3 f). The total number of proteins in the PPI network is N=50 and the total number of interactions between them is L=36. Twenty-two proteins from the dataset had no PPI data available (isolated nodes). In Figure 3 f, node size is proportional to the number of interactions of each node (k, degree). CUL3 (k=11), YBX1 (k=11), and CSNK1A1 (k=4) were the proteins with higher degree of connectivity in the network. Not considering the isolated nodes, the average number of neighbours in the network was 2,571. The mean clustering coefficient was *C*=0,247. The clustering coefficient characterizes how nearest neighbouring nodes of a node are connected to each other. If all of them are tightly connected to each other, then they form a clique and the clustering coefficient is 1. For a sparse random uncorrelated network of finite size *N*, this coefficient is close to zero. Note that the value C=0,247 is about 10 times larger than the clustering coefficient expected for a sparse random uncorrelated network (in the latter case $C = \langle q \rangle / N \sim 0.02$).

Twenty-nine proteins identified as PP1γ2-CT interactors presented PP1-binding motifs (purple outline in Figure 3 f; Supplementary Table 17) and 10 are testis/sperm-enriched/specific proteins (square nodes in Figure 3 f). All proteins, except PUSL1 and YBX3 were previously identified in human sperm proteomes (compiled by (55)). Fifteen proteins (YBX2, YBX3 H1FNT, SEMG1, PRSS37, HIST1H2BA, PSME4, SEMG2, ACR, GPX4, PPP1CC, SERPINA5, PA2G4, ZPBP2 and KLHL10) were associated with male infertility phenotypes. Twelve proteins were previously reported as involved in sperm motility regulation (blue nodes in Figure 3 f) and 3 in sperm-egg recognition and binding of sperm to zona-pellucida (pink nodes in Figure 3 f).

Discussion

It is known that reversible protein phosphorylation is essential for sperm motility and that PP1 is a key player in this process (7,10,11). High PP1 activity is inversely correlated with sperm motility such that inhibition of PP1 catalytic activity results in motility initiation in immotile sperm and increased kinetic activity of motile sperm (10,11). PP1 catalytic activity, substrate specificity and subcellular localization are controlled by myriad regulatory subunits (RIPPOs). One of the major set-backs for the design of selective modulators for PP1 lies in the similarity of the catalytic pocket between PP1 and other serine/threonine phosphatases (29). A more attractive approach to modulate sperm motility is to target the interaction interfaces between PP1 and RIPPOs using disruptive peptides. In 1997, Egloff and colleagues, used a short peptide based on the RIPPO p53BP2 to disrupt PP1/PPP1R2 interaction *in vitro* (56) and Chatterjee and colleagues showed that peptides based on the RVxF motif can, *in vivo*, release PP1 from several interactors and restore PP1 activity (29). More recently, treatment of human diseased myocardium with a PP1 disrupting peptide was shown to had an antiarrhythmic effect (57).

In this study, we demonstrated that a peptide which mimics the PP1 binding motif RVxF in AKAP4, a sperm-specific RIPPO, and its flanking sequences covalently coupled to penetratin (AKAP4-BM bioportide) was successfully delivered to sperm cells to significantly decrease sperm motility (Figure 1). Molecular modelling studies of the PP1/AKAP4 interaction facilitated the identification of the AKAP4-mimetic sequence YRSVITFVAV as an optimized binding sequence and enabled the development of an optimized Modified Stop Sperm (MSS1) bioportide with reduced size and increased potency of action (Figure 1; Table 1). The ability of MSS1 to disrupt the PP1γ2/AKAP4 complex *in vitro* confirmed a dominant-negative mode of action of this bioportide (Figure 1).

To further corroborate the general utility of the bioportide technology in modulating sperm motility, we also designed a bioportide to mimic the pentapetide PPP1R2 RVxF binding site (KSQKW) and flanking 7 AA sequences. This 19AA sequence was covalently coupled to the C105Y CPP to affect delivery into the sperm flagellum. *In vitro* studies proved that PPP1R2-BM bioportide disrupted PP1γ2/PPP1R2 interaction restoring PP1γ2 activity (Figure 2). Also, the fact

that half the amount of PPP1R2-BM released PP1γ2 from PPP1R2 inhibition suggests that the peptide has a high affinity towards PP1γ2 RVxF pocket. These results indicate that PPP1R2-BM competitively binds to PP1, displacing PPP1R2 and thereby increasing PP1γ2 activity. Surprisingly, the scrambled PPP1R2-BMsc bioportide also restored PP1γ2 activity (Figure 2). PPP1R2-BMsc presents a scrambled RVxF motif (QWKKS) which computational studies revealed to result in a higher structural stability and affinity towards the PP1 RVxF pocket. This unexpected finding explains the observed biological effect of this scrambled bioportide (Figure 2). Both PPP1R2-BM and PPP1R2-BMsc significantly decreased the percentage of fast motile sperm with a corresponding and increase in the percentage of immotile sperm (Figure 2).

Although PP1 isoforms typically display similar functional properties, the fact that they are differentially expressed and have a specific set of protein interactors hints that they can perform distinct and cell-type specific functions. This feature is evident in PP1γ isoform knockout studies, where the expression of other PP1 isoforms can compensate for the absence of PP1γ in every tissue except for the testis, rendering males infertile (13). More recently, it was confirmed that the spermatogenic defects observed in the global *Ppp1cc* knockout mice were specifically due to compromised PP1γ2 function (14,58) and that transgenic PP1γ1 expression and absence of PP1γ2 in *Ppp1cc* null mice, resulted in normal spermatogenesis but PP1γ2 was required for normal sperm function, specifically sperm motility (59). Specifically, the sperm localization of PP1γ1 in the transgenic mice and the association with RIPPOs were altered (59). Here we showed that a peptide that mimics the unique 22-amino acid C-terminus of PP1γ2 coupled with a CPP was able to penetrate the sperm cell to significantly decrease sperm motility (Figure 3). We hypothesize that the PP1γ2-CT peptide competes with isoform-specific interactors potentially involved in the targeting/inhibition of this phosphatase, affecting its action and, consequently, spermatozoa motility. Endophilin B1t, a testis enriched isoform of the somatic endophilin B1a, and the spermatogenic zip protein (Spz1) represent two PP1γ2 isoform-specific interactors previously identified (60,61). Both endophilin B1t and Spz1 do not interact with other PP1 isoforms or with a truncated PP1γ2 mutant lacking the unique C-terminus. Endophilin B1t and Spz1 were

previously shown to specifically inhibit PP1γ2 isoform activity (60,61). As stated previously, PP1 inhibition is essential for sperm motility. To identify other PP1γ2-specific interactors and elucidate the mechanism of action of PP1γ2-CT bioportide in inhibiting sperm motility, the interactome of the PP1γ2-CT bioportide was performed in human spermatozoa. Of the 50 PP1γ2-CT interactors identified by LC-MS/MS, 12 were identified as associated with regulation of sperm motility (blue nodes in Figure 3 f). Additionally, PP1γ2 localization in the sperm equatorial region suggests a role in sperm-egg interaction. In fact, TMEM225, a protein predominantly localized to the equatorial segment in mature spermatozoa of mice, was previously described as an interactor and inhibitor of PP1γ2 (62). Here we identified 3 proteins as PP1γ2-CT interactors that are involved in sperm-egg recognition and binding of sperm to zona-pellucida (pink nodes in Figure 3 f).

In conclusion, these studies indicate that proteomimetic bioportides can enter endocytosis-incompetent human sperm cells to modulate the activity of the testis- and sperm-specific protein PP1γ2 and so reduce sperm motility, a key prognostic indicator of male fertility. Although a marked decrease on sperm motility was achieved, motility was not completely abolished. To completely abolish sperm motility, we believe a multi-interaction interface targeting approach can be undertaken by combining bioportides targeting the RVxF-binding site, such as MSS1, and a bioportide mimetic of the unique C-terminus of PP1γ2. Also, the biochemical optimisation of the bioportides is likely to generate more efficacious lead compounds for clinical evaluation. For instance, to improve the stability of the optimized MSS1 (YRSVITFVAV), residues flanking the SVITF binding motif could be substituted with non-natural isosteres and D-amino acids. Retro, inverso and retro-inverso strategies, common structural modifications of bioactive peptides, are equally compatible with bioportide technologies. Individually and collectively, such modifications are likely to enhance both the pharmacodynamic and pharmacokinetic properties of next-generation Stop Sperm bioportides. Given that CPPs demonstrate an inherent lack of target specificity, it is also necessary to employ strategies to achieve sperm-specific delivery for clinical applications (36). Phage display technologies have generated several high-affinity cell-

and tissue-Homing Peptides which can be incorporated into bioportides as N- or C-terminal extensions or via a flexible linker (63). The modular nature of the Stop Sperm peptides will facilitate the synthesis of chimeric sequences modified by the inclusion of sperm-selective homing sequences to enable targeting in vivo.

Table 1 - Designation, sequence and molecular masses of the bioportides designed in this study**.** Underlined are the CPPs, penetratin (RQIKIWFQNRRMKWKK) or C105Y (CSIPPEVKFNKPFVYLI); PP1 binding motif are in bold (pattern in AKAP4: [RK]-X(0,1)-[VI]-{P}-[FW]; pattern in PPP1R2: K-S-Q-K-W). In italic are the RVxF flanking sequences. Peptide masses (M+ H+) were confirmed by MALDI time of flight mass spectrometry. To enable quantitative and qualitative uptake studies, peptides were extended with TAMRA fluorophore. [1]The last AA of PP1γ2 C-terminus (glutamic acid) was excluded due to its negative charge. All peptides were synthesized as C-terminal amides.

Peptide Designation	**Sequence**	**Mass (g/mol)**
AKAP4-BM	*GQQDQDR*^{40}***KVICF***^{45}*VAVSTLNV*^{53}*RQIKIWFQNRRMKWKK*	4448.3
AKAP4-BMmut	*GQQDQDR*^{40}***AAAAA***^{45}*VAVSTLNV*^{53}*RQIKIWFQNRRMKWKK*	4212.9
PPP1R2-BM	*VDEELSK*^{44}**KSQKW**^{48}*DEMNILA*^{54}CSIPPEVKFNKPFVYLI	4239.0
PPP1R2-BMsc	*VDEELSK*^{44}**QWKKS**^{48}*DEMNILA*^{54}CSIPPEVKFNKPFVYLI	4239.0
PP1γ2-CT[1]	RQIKIWFQNRRMKWKKKPNATRPVTPPRVASGLNPSIQKASNYRNNTVLY	5953.0
MSS1	*YRSVITFVAV*RQIKIWFQNRRMKWKK	3382.1

Figure legends

Figure 1 – Intracellular accumulation and impact on human sperm vitality and motility of the AKAP4-BM bioportides and molecular dynamics simulations and impact of the MSS1 bioportide in PP1γ2-AKAP4 complex and human sperm motility a) Microscopic evaluation of the intracellular accumulation of the AKAP4-BM bioportides in human spermatozoa: sperm cells were incubated for 1h with 10 µM TAMRA-labeled AKAP4-BM and AKAP4-BMmut (data not shown) and subsequently treated with 1% (w/v) trypsin. Negative control without the TAMRA-labeled peptides was performed and presented no reactivity (data not shown). Images are representative from three independent experiments. **b)** Quantitative analysis of AKAP4-BM and AKAP4-BMmut translocation into spermatozoa: sperm cells were incubated with TAMRA-labeled peptides (5 µM) for the times indicated (left); Sperm cells were incubated with 5 µM, 7,5 µM and 10 µM of TAMRA-labeled peptides for 15 min (right). Three independent experiments were performed in triplicated . Data are expressed as mean fluorescence (minus negative control). **c and d)** Impact of the peptides treatment (10 µM) in human sperm (c) vitality and (d) motility. Graph bars represent the mean values of three independent experiments performed in triplicate. Error bars 95% CI. Statistically significant findings are indicated with a (*). * $P<0.05$; ** $P<0.01$. **e)** 500 ns simulation of PP1γ protein. Snapshot of the predominant conformation cluster of MD simulation (90%) (grey), blue spheres indicate the RVxF binding pocket. **f)** RMSF showed high stability at the RVxF pocket residues161, 164, 237, 238, 250, 252, 256, 259, 261, 278, 283, 284, 286, 288, 290, 291 (grey boxes). **g)** Superimposition of **PP1γ**-AKAP4-Pep3 complex retrieved from the best ranked result of PinaColada. **h)** Impact of the MSS1 bioportide in PP1γ2-AKAP4 complex. PP1γ2 protein was resolved by SDS-PAGE and the membranes overlaid with either recombinant AKAP4 protein (25 pmol/mL) or MSS1 peptide (500 pmol/mL) and recombinant AKAP4 protein (25 pmol/mL). The binding was detected with anti-AKAP4 antibody. AKAP4 fluorescent signal was normalized to Ponceau S. Graph bars represent the mean values of 3 independent experiments. **i and j)** Impact of the MSS1 bioportide (10 µM) in human sperm motility. Graph bars represent the mean values of 3 independent experiments performed in

triplicate. Error bars 95% CI. * p<0.05; ** p<0.01. NC, negative control; MF, mean fluorescence; AU, arbitrary units.

Figure 2 – Effect of PPP1R2-BM bioportides towards disrupting PP1γ2/PPP1R2 complex, intracellular accumulation of the PPP1R2-BM bioportide in sperm, impact of PPP1R2-BM bioportide on sperm vitality and motility and molecular dynamics simulations on affinity and stability of PPP1R2-BM bioportide towards PP1 RVxF pocket. a) Comparison of phosphatase activity of PP1γ2 and PP1γ2/PPP1R2/PPP1R2-BM peptides. Data is expressed as arbitrary units of phosphatase activity (minus negative control). Graph bars and lines represent the mean values of 4 replicas. Error bars represent the SEM (standard error of the mean). Statistically significant findings are indicated with a (*). * P<0.05. **b)** Microscopic evaluation of the intracellular accumulation of the bioportides: sperm cells were incubated for 1h with 10 μM TAMRA-labeled peptides and subsequently treated with 1% (w/v) trypsin. Negative control without the TAMRA-labeled peptides was performed and presented no reactivity (data not shown). Images are representative from three independent experiments. **c)** Quantitative analysis of peptide translocation into human and bovine spermatozoa: sperm cells were incubated with TAMRA-labeled PPP1R2-BM or PPP1R2-BMsc (10μM) for 1h. The experiment was performed in triplicate in two different bulls or human samples. Data are expressed as mean fluorescence (minus negative control). Error bars represent the SEM (standard error of the mean). **d-e)** Impact of the-PPP1R2-BM peptides treatment (100 μM) in bovine spermatozoa (d) vitality and (e) motility. Graph bars represent the mean values of three independent experiments performed in triplicate. Error bars 95% CI. * P<0.05; ** P<0.01. NC, negative control. **f)** Molecular dynamics of PPP1R2-BM and PPP1R2-BMsc peptide. RVxF and the 7 flanking AA of the PPP1R2-BM peptide. **g)** Scrambled RVxF and the 7 flanking AA of the PPP1R2-BMsc bioportide. Note that the number of the AA correspond to their position within the peptide not within PPP1R2. Green: N-terminus; Orange: C-terminus; Blue: RVxF AA side chains. **h)** AA substitution studies of RVxF motif. The substitutions studies were performed using previous experimental data on PP1/PPP1R2 interaction. The more negative the △affinity and △stability (kcal/mol), the stronger the affinity and stability, respectively. *In the scrambled peptide, the lysine present at position 47

was not changed. In the substitutions studies this lysine was changed for an alanine. MF, mean fluorescence; AU, arbitrary units.

Figure 3 – Intracellular accumulation of the PP1γ2-CT peptide in human sperm, impact on human sperm vitality and motility and protein-protein interaction network of the PP1γ2-CT peptide. a) Microscopic evaluation of the intracellular accumulation of the PP1γ2-CT bioportide in human sperm: sperm cells were incubated for 1h with 10 μM TAMRA-labeled peptide and subsequently treated with 1% (w/v) trypsin. Negative control without the TAMRA-labeled peptide was performed and presented no reactivity (data not shown). Images are representative from three independent experiments. **b)** Quantitative analysis of peptide translocation into spermatozoa: sperm cells were incubated with TAMRA-labeled PP1γ2-CT (5 μM) for the times indicated (left); sperm cells were incubated with 5 μM, 7,5 μM and 10 μM of TAMRA-labeled PP1γ2-CT for 15 min (right). Three independent experiments were performed in triplicate. Data are expressed as mean fluorescence (minus negative control). **c-e)** Impact of the PP1γ2-CT bioportide treatment (10 μM) in human spermatozoa (c) vitality and (d and e) motility. Graph bars represent the mean values of three independent experiments performed in triplicate. Error bars 95% CI. Statistically significant findings are indicated with a (*). * $P<0.05$; ** $P<0.01$. NC, negative control; MFI, mean fluorescence intensity; AU, arbitrary units. f) **Protein-protein interaction network of the PP1γ2-CT peptide interactors.** Purple outline represents proteins presenting PP1-binding motifs. Green nodes represent the proteins previously identified as PP1γ interactors. Blue nodes represent proteins associated with sperm motility. Pink nodes represent the proteins associated with sperm-egg recognition and binding of sperm to zona-pellucida. Square nodes represent testis/sperm-enriched/specific proteins. Node sizes represent relative degree of the nodes. Proteins are represented by gene name. PP1γ (PPP1CC), shown in yellow, was considered since PPI information for the different alternative splicing isoforms is not available.

Funding

This work was supported by FEDER funds through the “Programa Operacional Competitividade e Internacionalização COMPETE 2020” and by National Funds through the FCT Fundação para a Ciência e Tecnologia (PTDB/BBB-BQB/3804/2014). We are thankful to iBiMED (UIDB/04501/2020 and POCI-01-0145-FEDER-007628) for supporting this project. This work was also supported by an individual grant from FCT to J.V.S. (SFRH/BPD/123155/2016).

Conflicts of Interest

Joana Vieira Silva, Maria João Freitas, Sarah Jones, John Howl and Margarida Fardilha have a filed patent (WO2019016555A1) on the PP1-disrupting peptides described in this manuscript.

References

1. Department of Economic and Social Affairs, Population Division F and FPS. World Contraceptive Use. 2018.
2. Bearak J, Popinchalk A, Alkema L, Sedgh G. Global, regional, and subregional trends in unintended pregnancy and its outcomes from 1990 to 2014: estimates from a Bayesian hierarchical model. Lancet Glob Heal 2018;6:e380–9.
3. Thirumalai A, Page ST. Recent Developments in Male Contraception. Drugs 2019;79:11–20.
4. Page ST, Amory JK. Male hormonal contraceptive — are we there yet? Nat Rev Endocrinol 2018;14:685–6.
5. WHO, CONRAD. Male Hormonal Contraceptive Trial Ending Early: CONRAD. 2011;
6. Arifuzzaman S, Rahman MS, Pang M-G. Research update and opportunity of non-hormonal male contraception: Histone demethylase KDM5B-based targeting. Pharmacol Res 2019;141:1–20.
7. Freitas MJ, Vijayaraghavan S, Fardilha M. Signaling mechanisms in mammalian sperm motility. Biol Reprod 2017;96:2–12.
8. Verbinnen I, Ferreira M, Bollen M. Biogenesis and activity regulation of protein phosphatase 1. Biochem Soc Trans 2017;45:89–99.
9. Fardilha M, Esteves SLC, Korrodi-Gregório L, da Cruz e Silva OAB, da Cruz e Silva FF. The physiological relevance of protein phosphatase 1 and its interacting proteins to health and disease. Curr Med Chem 2010;17:3996–4017.
10. Smith GD, Wolf DP, Trautman KC, da Cruz e Silva EF, Greengard P, Vijayaraghavan S. Primate sperm contain protein phosphatase 1, a biochemical mediator of motility. Biol Reprod 1996;54:719–27.
11. Vijayaraghavan S, Stephens DT, Trautman K, Smith GD, Khatra B, da Cruz e Silva EF, et al. Sperm motility development in the epididymis is associated with decreased glycogen synthase kinase-3 and protein phosphatase 1 activity. Biol Reprod 1996;54:709–18.
12. Smith GD, Wolf DP, Trautman KC, Vijayaraghavan S. Motility potential of macaque epididymal sperm: the role of protein phosphatase and glycogen synthase kinase-3 activities. J Androl 20:47–53.
13. Varmuza S, Jurisicova A, Okano K, Hudson J, Boekelheide K, Shipp EB. Spermiogenesis is impaired in mice bearing a targeted mutation in the protein phosphatase 1cgamma gene. Dev Biol 1999;205:98–110.
14. Sinha N, Pilder S, Vijayaraghavan S. Significant Expression Levels of Transgenic PPP1CC2 in Testis and Sperm Are Required to Overcome the Male Infertility Phenotype of Ppp1cc Null Mice. PLoS One 2012;7.
15. Gregorio LK, Esteves SLC, Fardilha M, Korrodi-Gregório L, Esteves SLC, Fardilha M, et al. Protein phosphatase 1 catalytic isoforms: specificity toward interacting proteins. Transl Res 2014;164:366–91.
16. Silva JV, Korrodi-Gregório L, Luers G, Cardoso MJ, Patrício A, Maia N, et al. Characterisation of several ankyrin repeat protein variant 2, a phosphoprotein phosphatase 1-interacting protein, in testis and spermatozoa. Reprod Fertil Dev 2015;
17. Browne GJ, Fardilha M, Oxenham SK, Wu W, Helps NR, da Cruz E Silva OAB, et al. SARP, a new alternatively spliced protein phosphatase 1 and DNA interacting protein. Biochem J 2007;402:187–96.
18. Fardilha M, Esteves SLC, Korrodi-Gregório L, Vintém AP, Domingues SC, Rebelo S, et al. Identification of the human testis protein phosphatase 1 interactome. In: Biochemical Pharmacology. 2011. p. 1403–15.
19. Korrodi-Gregorio L, Vieira SI, Esteves SLC, Silva J V, Freitas MJ, Brauns A-KK, et al. TCTEX1D4, a novel protein phosphatase 1 interactor: connecting the phosphatase to the microtubule network. Biol Open 2013;2:453–65.
20. Korrodi-gregório L, Ferreira M, Vintém AP, Wu W, Muller T, Marcus K, et al. Identification and characterization of two distinct PPP1R2 isoforms in human

spermatozoa. 2013;
21. Wu D, De Wever V, Derua R, Winkler C, Beullens M, Van Eynde A, et al. A substrate-trapping strategy for protein phosphatase PP1 holoenzymes using hypoactive subunit fusions. J Biol Chem 2018;293:15152–62.
22. Ceulemans H, Bollen M. Functional diversity of protein phosphatase-1, a cellular economizer and reset button. Physiol Rev 2004;84:1–39.
23. Silva JV, Yoon S, De Bock P-J, Goltsev A V., Gevaert K, Mendes JFF, et al. Construction and analysis of a human testis/sperm-enriched interaction network: Unraveling the PPP1CC2 interactome. Biochim Biophys Acta - Gen Subj 2017;1861:375–85.
24. Moretti E, Scapigliati G, Pascarelli NA, Baccetti B, Collodel G. Localization of AKAP4 and tubulin proteins in sperm with reduced motility. Asian J Androl 2007;9:641–9.
25. Miki K, Willis WD, Brown PR, Goulding EH, Fulcher KD, Eddy EM. Targeted disruption of the Akap4 gene causes defects in sperm flagellum and motility. Dev Biol 2002;248:331–42.
26. Huang Z, Somanath PR, Chakrabarti R, Eddy EM, Vijayaraghavan S. Changes in intracellular distribution and activity of protein phosphatase PP1gamma2 and its regulating proteins in spermatozoa lacking AKAP4. Biol Reprod 2005;72:384–92.
27. Hendrickx A, Beullens M, Ceulemans H, Den Abt T, Van Eynde A, Nicolaescu E, et al. Docking motif-guided mapping of the interactome of protein phosphatase-1. Chem Biol 2009;16:365–71.
28. Heroes E, Lesage B, Görnemann J, Beullens M, Van Meervelt L, Bollen M. The PP1 binding code: A molecular-lego strategy that governs specificity. FEBS J. 2013;280:584–95.
29. Chatterjee J, Beullens M, Sukackaite R, Qian J, Lesage B, Hart DJ, et al. Development of a peptide that selectively activates protein phosphatase-1 in living cells. Angew Chemie - Int Ed 2012;51:10054–9.
30. Ammosova T, Platonov M, Yedavalli VRK, Obukhov Y, Gordeuk VR, Jeang K-T, et al. Small Molecules Targeted to a Non-Catalytic "RVxF" Binding Site of Protein Phosphatase-1 Inhibit HIV-1. PLoS One 2012;7:e39481.
31. Trebacz M, Wang Y, Makotta L, Henschke L, Köhn M. Development of a Photoactivatable Protein Phosphatase-1-Disrupting Peptide. J Org Chem 2020;85:1712–7.
32. Wang Y, Hoermann B, Pavic K, Trebacz M, Rios P, Köhn M. Interrogating PP1 Activity in the MAPK Pathway with Optimized PP1-Disrupting Peptides. ChemBioChem 2019;20:66–71.
33. Jones S, Lukanowska M, Suhorutsenko J, Oxenham S, Barratt C, Publicover S, et al. Intracellular translocation and differential accumulation of cell-penetrating peptides in bovine spermatozoa: evaluation of efficient delivery vectors that do not compromise human sperm motility. Hum Reprod 2013;28:1874–89.
34. Dinca A, Chien W-M, Chin M. Intracellular Delivery of Proteins with Cell-Penetrating Peptides for Therapeutic Uses in Human Disease. Int J Mol Sci 2016;17:263.
35. Howl J, Matou-Nasri S, West DC, Farquhar M, Slaninová J, Östenson CG, et al. Bioportide: An emergent concept of bioactive cell-penetrating peptides. Cell Mol Life Sci 2012;69:2951–66.
36. Howl J, Jones S. Insights into the molecular mechanisms of action of bioportides: a strategy to target protein-protein interactions. Expert Rev Mol Med 2015;17:e1.
37. Lukanowska M, Howl J, Jones S. Bioportides: Bioactive cell-penetrating peptides that modulate cellular dynamics. Biotechnol. J. 2013;8:918–30.
38. Howl J, Jones S. Protein Mimicry and the Design of Bioactive Cell-Penetrating Peptides. In: Langel Ü, editor. Cell-Penetrating Peptides: Methods and Protocols. New York: Springer; 2015. p. 177–90.
39. Palasek SA, Cox ZJ, Collins JM. Limiting racemization and aspartimide formation in microwave-enhanced Fmoc solid phase peptide synthesis. J Pept Sci 2007;13:143–8.
40. Jones S, Osman S, Howl J. A High-Throughput Synthetic Platform Enables the

Discovery of Proteomimetic Cell Penetrating Peptides and Bioportides. Int J Pept Res Ther 2019;25:1–8.
41. Jones S, Martel C, Belzacq-Casagrande AS, Brenner C, Howl J. Mitoparan and target-selective chimeric analogues: Membrane translocation and intracellular redistribution induces mitochondrial apoptosis. Biochim Biophys Acta - Mol Cell Res 2008;1783:849–63.
42. Holm T, Johansson H, Lundberg P, Pooga M, Lindgren M, Langel U. Studying the uptake of cell-penetrating peptides. Nat Protoc 2006;1:1001–5.
43. Iqbal M, Aleem M, Ijaz A, Rehman H, Yousaf MS. Assessment of buffalo semen with the 3-(4,5-dimethylthiazol-2-yl)-2,5-diphenyltetrazolium bromide reduction assay. J Anim Sci 2010;88:922–5.
44. Case D, Darden T, Cheatham T, Simmerling C, Wang J, Duke R, et al. AMBER 14. San Francisco: 2014.
45. Maier JA, Martinez C, Kasavajhala K, Wickstrom L, Hauser KE, Simmerling C. ff14SB: Improving the Accuracy of Protein Side Chain and Backbone Parameters from ff99SB. J Chem Theory Comput 2015;11:3696–713.
46. Berendsen HJC, Postma JPM, van Gunsteren WF, DiNola A, Haak JR. Molecular dynamics with coupling to an external bath. J Chem Phys 1984;81:3684–90.
47. Daura X, van Gunsteren WF, Mark AE. Folding-unfolding thermodynamics of a ?-heptapeptide from equilibrium simulations. Proteins Struct Funct Genet 1999;34:269–80.
48. Dorigo M, Gambardella LM. Ant colony system: a cooperative learning approach to the traveling salesman problem. IEEE Trans Evol Comput 1997;1:53–66.
49. Donsky E, Wolfson HJ. PepCrawler: A Fast RRT–Like Algorithm for High–Resolution Refinement and Binding–Affinity Estimation of Peptide Inhibitors. In: T.M. P, MF S, editors. Algorithms in Bioinformatics. Berlin, Heidelberg: Springer; 2011. p. 73–5.
50. Jorgensen WL, Chandrasekhar J, Madura JD, Impey RW, Klein ML. Comparison of simple potential functions for simulating liquid water. J Chem Phys 1983;79:926–35.
51. Schrödinger LCC. Maestro. 2014;
52. Shannon P, Markiel A, Ozier O, Baliga NS, Wang JT, Ramage D, et al. Cytoscape: A software Environment for integrated models of biomolecular interaction networks. Genome Res 2003;13:2498–504.
53. Zaidman D, Wolfson HJ. PinaColada: peptide–inhibitor ant colony ad-hoc design algorithm. Bioinformatics 2016;32:2289–96.
54. Keilhauer EC, Hein MY, Mann M. Accurate Protein Complex Retrieval by Affinity Enrichment Mass Spectrometry (AE-MS) Rather than Affinity Purification Mass Spectrometry (AP-MS). Mol Cell Proteomics 2015;14:120–35.
55. Santiago, Silva, Fardilha, Santiago J, Silva JV, Fardilha M. First Insights on the Presence of the Unfolded Protein Response in Human Spermatozoa. Int J Mol Sci 2019;20:5518.
56. Egloff M-P. Structural basis for the recognition of regulatory subunits by the catalytic subunit of protein phosphatase 1. EMBO J 1997;16:1876–87.
57. Fischer TH, Eiringhaus J, Dybkova N, Saadatmand A, Pabel S, Weber S, et al. Activation of protein phosphatase 1 by a selective phosphatase disrupting peptide reduces sarcoplasmic reticulum Ca 2+ leak in human heart failure. Eur J Heart Fail 2018;20:1673–85.
58. Sinha N, Puri P, Nairn AC, Vijayaraghavan S. Selective ablation of Ppp1cc gene in testicular germ cells causes oligo-teratozoospermia and infertility in mice. Biol Reprod 2013;89:128.
59. Dudiki T, Joudeh N, Sinha N, Goswami S, Eisa A, Kline D, et al. The protein phosphatase isoform PP1γ1 substitutes for PP1γ2 to support spermatogenesis but not normal sperm function and fertility†. Biol Reprod 2019;100:721–36.
60. Hrabchak C, Varmuza S. Identification of the spermatogenic zip protein Spz1 as a putative protein phosphatase-1 (PP1) regulatory protein that specifically binds the PP1c??2 splice variant in mouse testis. J Biol Chem 2004;279:37079–86.
61. Hrabchak C, Henderson H, Varmuza S. A testis specific isoform of endophilin B1, endophilin B1t, interacts specifically with protein phosphatase-1c??2 in mouse testis and

is abnormally expressed in PP1c?? Null Mice. Biochemistry 2007;46:4635–44.
62. Matsuura M, Yogo K. TMEM225: A possible protein phosphatase 1γ2 (PP1γ2) regulator localizes to the equatorial segment in mouse spermatozoa. Mol Reprod Dev 2015;82:139–48.
63. Zahid M, Robbins P. Cell-Type Specific Penetrating Peptides: Therapeutic Promises and Challenges. Molecules 2015;20:13055–70.

Figure 1

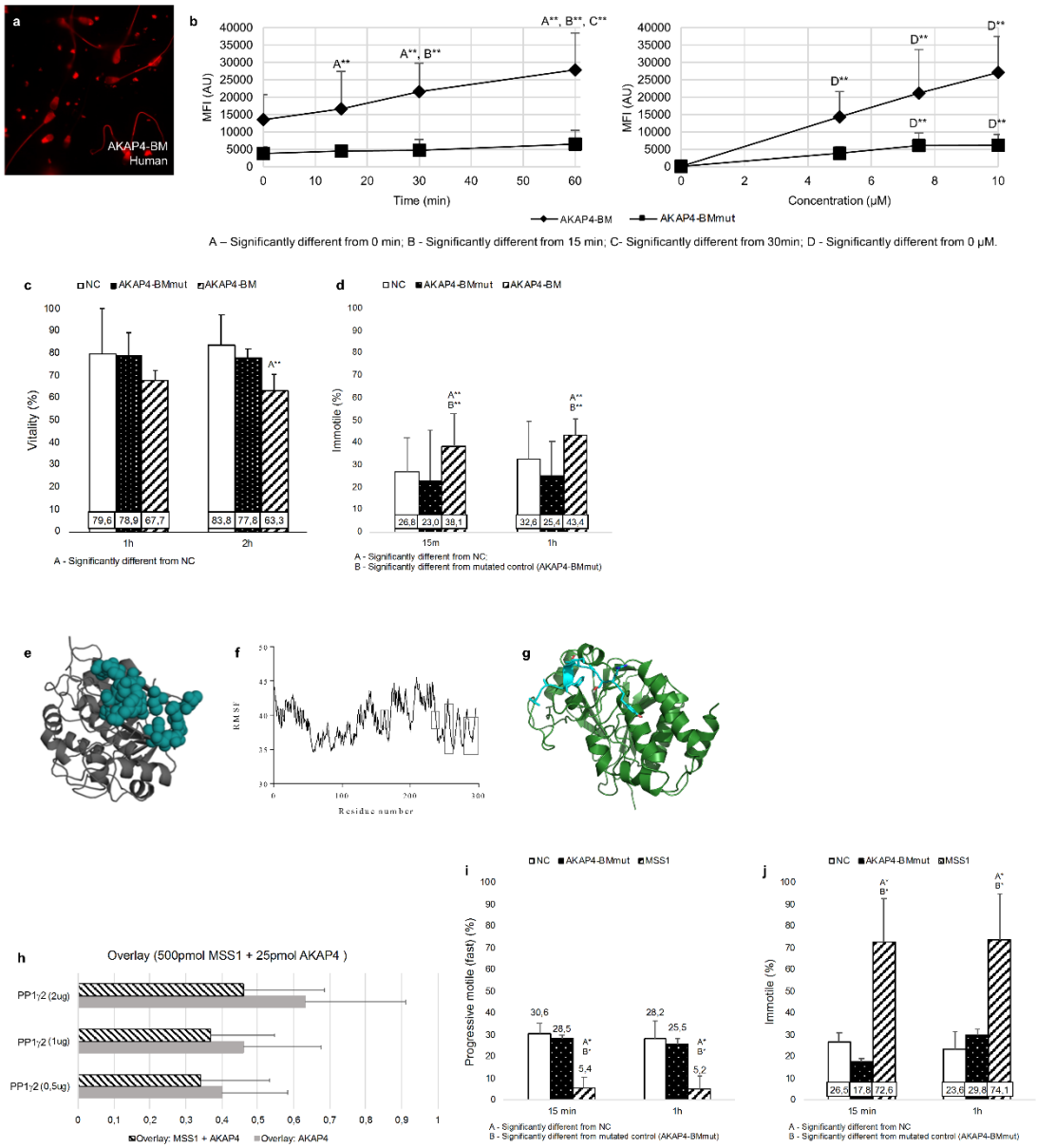
a
AKAP4-BM
Human
b
MFI (AU)
Time (min)
A**
A**, B**
A**, B**, C**
Concentration (µM)
D**
AKAP4-BM
AKAP4-BMmut
A – Significantly different from 0 min; B - Significantly different from 15 min; C- Significantly different from 30min; D - Significantly different from 0 µM.
c
NC
AKAP4-BMmut
AKAP4-BM
Vitality (%)
79,6
78,9
67,7
83,8
77,8
63,3
1h
2h
A - Significantly different from NC
d
Immotile (%)
26,8
23,0
38,1
32,6
25,4
43,4
15m
1h
A - Significantly different from NC;
B - Significantly different from mutated control (AKAP4-BMmut)
e
f
RMSF
Residue number
g
h
Overlay (500pmol MSS1 + 25pmol AKAP4)
PP1γ2 (2ug)
PP1γ2 (1ug)
PP1γ2 (0,5ug)
Overlay: MSS1 + AKAP4
Overlay: AKAP4
i
MSS1
Progressive motile (fast) (%)
30,6
28,5
5,4
28,2
25,5
5,2
15 min
1h
A - Significantly different from NC
B - Significantly different from mutated control (AKAP4-BMmut)
j
Immotile (%)
26,5
17,8
72,6
23,6
29,8
74,1
A - Significantly different from NC
B - Significantly different from mutated control (AKAP4-BMmut)

Figure 2

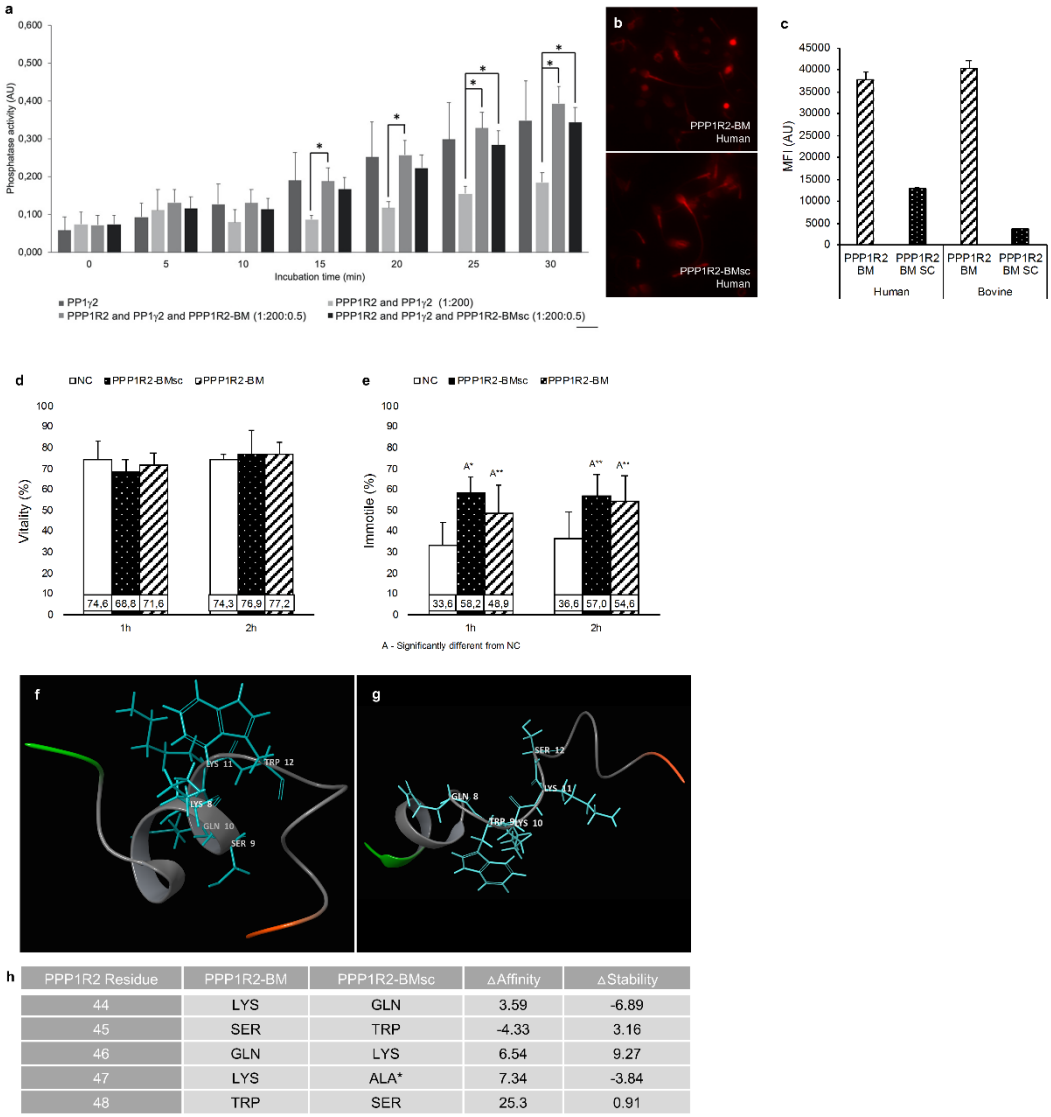

h

PPP1R2 Residue	PPP1R2-BM	PPP1R2-BMsc	ΔAffinity	ΔStability
44	LYS	GLN	3.59	-6.89
45	SER	TRP	-4.33	3.16
46	GLN	LYS	6.54	9.27
47	LYS	ALA*	7.34	-3.84
48	TRP	SER	25.3	0.91

Figure 3

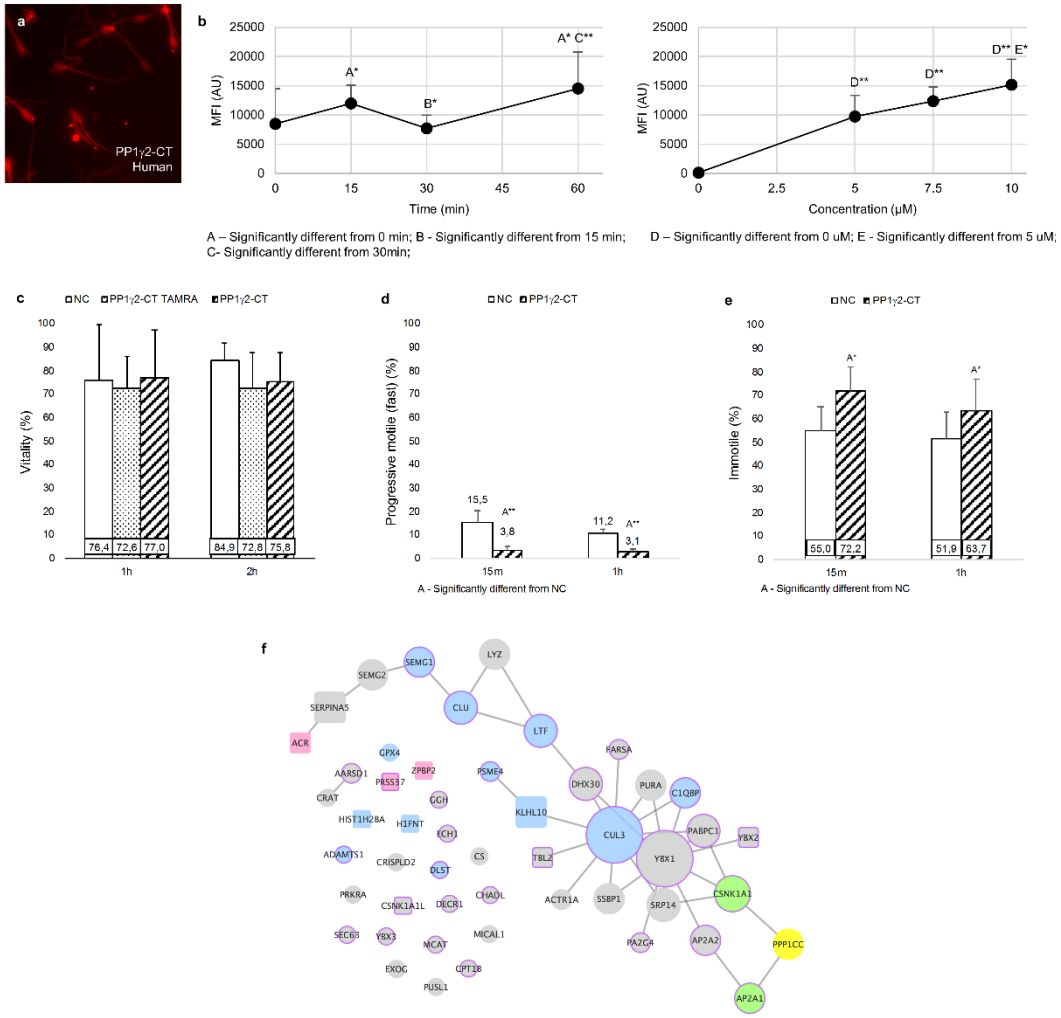
a
PP1γ2-CT
Human
b
MFI (AU)
Time (min)
A* C**
A*
B*
Concentration (μM)
D** E*
D**
D**
A – Significantly different from 0 min; B - Significantly different from 15 min;
C- Significantly different from 30min;
D – Significantly different from 0 uM; E - Significantly different from 5 uM;
c
NC
PP1γ2-CT TAMRA
PP1γ2-CT
Vitality (%)
76,4
72,6
77,0
84,9
72,8
75,8
1h
2h
d
NC
PP1γ2-CT
Progressive motile (fast) (%)
15,5
A**
3,8
11,2
A**
3,1
15m
1h
A - Significantly different from NC
e
NC
PP1γ2-CT
Immotile (%)
A*
A*
55,0
72,2
51,9
63,7
15m
1h
A - Significantly different from NC
f
LYZ
SEMG1
SEMG2
SERPINA5
CLU
LTF
ACR
GPX4
FARSA
AARSD1
PRSS37
ZPBP2
PSME4
DHX30
PURA
C1QBP
CRAT
GGH
KLHL10
HIST1H2BA
H1FNT
ECH1
CUL3
PABPC1
YBX2
ADAMTS1
CRISPLD2
CS
TBL2
YBX1
DLST
PRKRA
CSNK1A1L
DECR1
CHADL
ACTR1A
SSBP1
SRP14
CSNK1A1
SEC63
YBX3
MCAT
MICAL1
PA2G4
AP2A2
PPP1CC
EXOG
CPT1B
PUSL1
AP2A1